arXiv:1210.5366v1 [cond-mat.mtrl-sci] 19 Oct 2012

An in-depth TEM/SAXS study of aging induced precipitation in MgZn

J. M. Rosalie [1] **and B. R. Pauw** [2]

[1] Structural Materials Unit, National Institute for Materials Science (NIMS), 1-2-1 Sengen, 305-0047, Tsukuba, Japan

E-mail: `rosalie.julianmark@nims.go.jp`
[2] International Center for Young Scientists (ICYS) National Institute for Materials Science (NIMS), 1-2-1 Sengen, 305-0047, Tsukuba, Japan

E-mail: `brian@stack.nl`

Abstract.

Nanoscale rod-like precipitate development observed during ageing of MgZn alloys is characterised in detail using a combination of transmission electron microscopy and small-angle x-ray scattering. Precipitate morphology and phase, width and length distribution as well as volume fraction have been carefully determined for nine different ageing times from the early stages of precipitation to well beyond the peak aged condition. These resulting structural parameters are correlated with physical parameters, in particular micro-hardness testing.

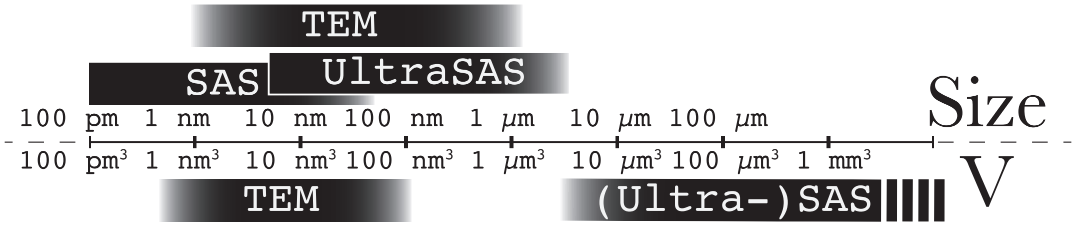

Figure 1. Typical size range of nanostructural features and sampling volume of transmission electron microscopy (TEM) and small-angle and ultra-small-angle scattering techniques (SAS/UltraSAS).

1. Introduction

Perfecting high-performance alloys through tuning of its nanostructure is the key to more efficient transportation and more advanced construction. Such optimization requires intricate knowledge of the interrelationships between nanostructure, processing and physical properties. Qualitative and quantitative characterization of the nanostructure is a key challenge in establishing these links.

Transmission Electron microscopy (TEM) is a very suitable and common technique for qualitative nanostructural scrutiny but unfortunately poorly suited for statistical, quantitative work due to the microscopic size of the observed volumes (Fig. 1). Small-angle scattering (SAS), on the other hand, statistically quantifies nanostructural parameters over large sample volumes with a minimum of sample preparation, but requires qualitative information on the structure to arrive at a non-ambiguous solution. As such, a symbiotic relationship can be exploited between TEM and SAS, with the strengths of the one supplanting the weaknesses of the other.

Previously, SAXS has been used to study precipitation in alloys, with several examples where the precipitates can be described as essentially globular in shape. These include Guinier-Preston zones (GPZ) in Al-Zn-Mg [1, 2, 3] and Al-Ag [4, 5, 6] alloys and spherical δ' precipitates in Al-Li alloys [7] and carbon steels [8].

Alloys containing globular precipitates, however, only account for a small proportion of all precipitation strengthened systems. The majority of precipitation-strengthened alloys contain precipitates of rod-, plate- or lath- like morphologies. In designing aluminium alloys for high-strength applications, for example, the precipitates should ideally be high aspect-ratio plates [9]. On a volume-fraction basis, such precipitates are shown to be more effective at impeding dislocation glide (a major contribution affecting most physical properties) than isotropic precipitates [9, 10, 11]. SAXS analysis of these systems is less numerous given the complexity of the data analysis, though several good examples do exist [12, 13].

The main challenge in the application of SAXS lies in the involved data interpretation required for extraction, which is most straightforward (but still cumbersome) for globular precipitates and well-defined precipitate size distributions [14].

Recently, however, a data collection and interpretation methodology has been refined based on a Monte-Carlo optimisation process, which is conceptually straightforward, allows determination of form-free particle size distributions, and theoretically can be easily extended to support a variety of particle shapes [15]. Provided sufficient morphological parameters are supplied to extract a unique solution (in particular overall particle shape and aspect ratio), it should allow for the study of rod-like precipitates.

Magnesium-zinc alloys are one example of a high-performance material intended for use in, amongst others, the automotive industry. Compositions based on this system are industrially important, forming the basis of the ZK (Mg-Zn-Zr) family of alloys. Their physical properties are highly correlated to the material nanostructure, with precipitates playing a key role. Establishing an accurate correlation between the precipitate morphology and the physical properties is therefore of utmost importance.

Magnesium-zinc alloys derive strength from a fine dispersion of high-aspect ratio rod-like particles (known as β_1' precipitates) that are aligned parallel to the hexagonal axis of the magnesium matrix [16]. Precipitation of these particles can be stimulated by rolling [17] or by tensile deformation to generate dislocations [18]. Magnesium alloys develop strong texture when plastically deformed via rolling or extrusion.

For this work, a magnesium-zinc alloy was extruded to generate a tube texture. The β_1' precipitates are examined using both TEM and small-angle X-ray scattering (SAXS) and supplemented by several other techniques. The resulting nanostructural details are employed to establish structure-property relationships.

2. Experimental

A binary magnesium-zinc alloy was prepared from high-purity elements by direct chill casting. A composition of Mg-3.4at.% Zn was measured by atomic emission spectroscopy. The billet was homogenised at 300°C for 24 h and extruded at 300°C with an extrusion ratio of 12:1 to form a 12 mm diameter rod. Samples were cut from this rod, encapsulated in argon, solution-treated at 300°C for 1 h and quenched into water at ambient temperature.

The microstructure and texture were examined in the solution-treated and quenched condition, using light microscopy and electron back scattered diffraction. Reflected light micrographs were obtained from ground and polished samples both in cross-section (ie. parallel to the extrusion direction (XD)) and longitudinal section (normal to the XD). An acetic-picral etchant was used to highlight the grain boundaries.

The texture of a solution-treated, cross-sectional sample was measured via electron back scattered diffraction (EBSD) using a field-emission scanning electron microscope (FE-SEM). Data was analysed using OIM Analysis software, version 6.1.

Subsequent testing was carried out on samples isothermally aged at 150°C in a silicon oil bath and quenched in water at ambient temperature. Previous studies reported maximum hardness for MgZn alloys after 48 h ageing at this temperature [18]. Ageing times in used this work were from 6 h (underaged) –406 h (significantly overaged).

The micro-indentation hardness of the alloy was measured at each ageing time. Samples cut in cross-section were removed from the oil bath, quenched and embedded in a low-temperature resin, ground and polished. The Vickers micro indentation hardness was measured using a Matsuzawa AMT-X7FS automated tester. Each test included a total of 16 measurements per sample using a load of 100 g (solution treated and quenched (STQ) i.e. 0 h ageing) or 200 g (all other samples).

2.1. SAXS measurements

SAXS measurements were performed on a laboratory instrument based around a rotating anode generator with a molybdenum target. Mo $k_{\alpha,1}$ emitted radiation was selected and focused using an Osmic confocal mirror. The incident beam was further collimated using three pinholes of 0.3, 0.2 and 0.45 mm in diameter, with the sample positioned immediately after the third pinhole. Nominal beam diameter at the sample position is estimated to be approximately 200 μm. The flightpath is a continuous vacuum from optics to detector. Foil thickness was approximately 0.6 mm. For detection of the scattered radiation, a Dectris Pilatus 100k detector was used in combination with a translation stage. For every measurement, three images are collected and stitched together to form a single square scattering image consisting of 487 by 497 pixels, each measuring 172 μm by 172 μm. The detector is placed 1.36 meter from the sample, its distance verified by ruler and measurement of a silver behenate standard, allowing for an angular coverage of 1×10^8 to 3.7×10^9 reciprocal meter (0.01 to 0.37 reciprocal Ångström, respectively) in q. q is defined as $q = 4\pi/\lambda \sin(\theta)$, where the radiation wavelength is denoted as λ, and 2θ is the scattering angle.

As detailed in a separate publication [15], collected data is corrected for natural background radiation, transmission, sample thickness, measurement time, primary beam flux, parasitic background, polarisation, detector solid angle coverage and sample self-absorption using in-house developed data reduction software written in the Python language. Deadtime correction is unnecessary at the count rates encountered in this study [19], and dead-pixel and flatfield corrections are performed by the detector acquisition software prior to ingestion by the data reduction software [20]. The intensity is subsequently binned using 200 bins spanning the aforementioned q range, and scaled to absolute units using a calibrated glassy carbon standard provided by [21]. Statistical uncertainty on the datapoints is set to the maximum of either: 1) The propagated Poisson counting statistics, 2) The sample standard deviation in the histogram bin, or 3) 1% of the intensity in the histogram bin (the realistically minimum achievable uncertainty given the aforementioned corrections). As the parasitic scattering is minimal through complete beam path evacuation, improved statistics have been obtained by skewing the time division between sample and background measurement to favor sample measurement time.

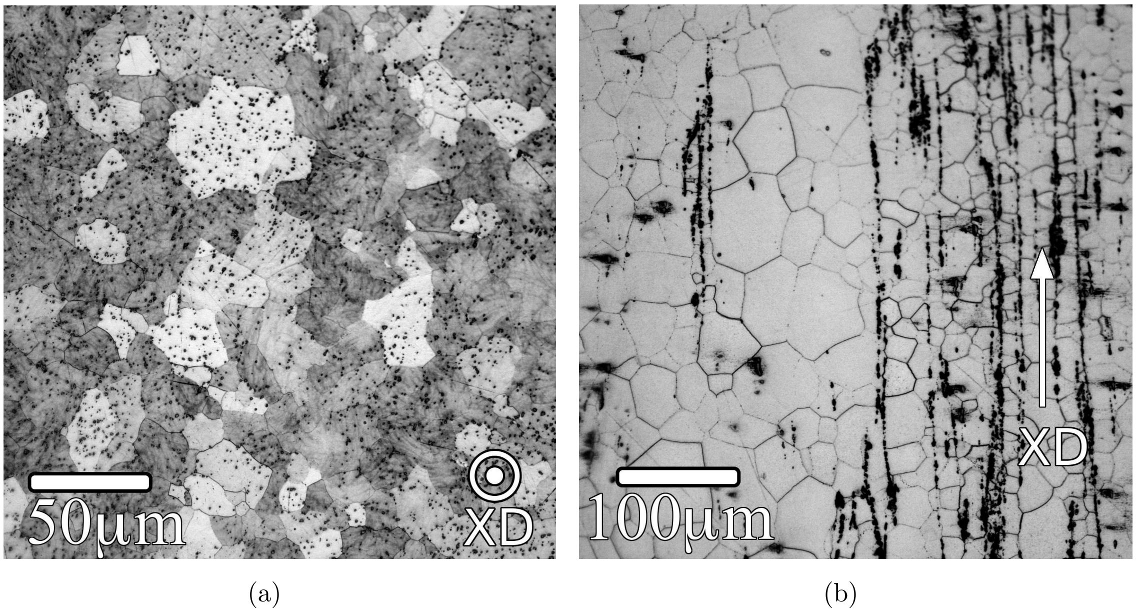

(a) (b)

Figure 2. Light micrographs of the solution treated and quenched Mg-Zn alloy. (a) show the microstructure viewed along the extrusion direction (XD). (b) shows the structure normal to the extrusion direction, which is indicated by an arrow.

2.2. Transmission electron microscopy

After the SAXS measurements were completed, TEM foils were prepared from the central portion of these samples. Discs (3 mm diameter) were punched from these samples, ground to ∼50–60 μm and thinned to perforation using a Gatan precision ion polisher.

Precipitate size and number density were measured using diffraction contrast transmission electron microscopy (TEM) using a JEM 2100 instrument operating at 200 kV. Foils were analysed at ageing times of 6, 24,192 and 406 h. The length, calliper diameter and aspect ratio were were determined with the electron beam aligned normal to the hexagonal axis of the Mg grains, (i.e. with the precipitate rods viewed side-on). The precipitate diameter was also measured with the electron beam along the hexagonal axis (i.e. with the precipitates in cross-section) (24 h and 406 h samples only).

3. Results

3.1. Microstructure and texture

Reflected light micrographs showed a microstructure consisting of equiaxed grains containing coarse intermetallic particles. Micrographs are shown in Figure 2(a) and when viewed in longitudinal section (Figure 2(b)) these particles are distributed in bands parallel to the extrusion direction. An average grain diameter of 17 μm with a standard deviation of 14 μm was determined from EBSD images.

The alloy had a fibre texture, as expected for extruded MgZn. A pole figure calculated showing the distribution of [0001] poles is provided in Figure 3(a). The extrusion direction lies at the centre of the stereogram, whereas the strongest intensity for [0001] poles of ∼4 is around the edges, i.e. at 90° to the XD ‡. This indicates that the [0001] axes of the Mg grains are radially distributed.

An inverse pole figure (IPF) for the XD is provided in Figure 3(b). This also shows a low intensity for [0001] poles, with an intensity in the XD of < 0.5. The strongest intensity of 2.765 was recorded close to the $\{2\overline{1}\overline{1}0\}$ plane normal.

The relationship between the orientation of the β_1' rods and the extruded material is shown schematically in Figure 3(c). As indicated in Figure 3(a),3(b) the Mg grains are aligned predominantly with the $[2\overline{1}\overline{1}0]$ poles close to the XD and the [0001] axes radially distributed. The long axis of the β_1' precipitates lie parallel to the [0001] axis of the magnesium grains, at an angle defined as φ to the XD. For the purposes of SAXS analysis the β_1' precipitates are regarded as cylindrical rods of radius r and half-length l.

The magnitude of the misorientation angle, φ, was measured by calculating the angle between the [0001] axis of the Mg grains and the XD, from the EBSD data using axis-angle notation. The distribution of misorientation angles is shown in Figure 3(d). The number fraction of grains with misorientation angle $< 30°$ is negligible and the highest proportion of grains have angles between 80–90°. The average angle between the hexagonal axis of the grains and the XD was 73.8°. This allows the distribution of β_1' precipitate to be regarded as having a radial distribution for the Monte Carlo simulation of the SAXS intensity.

3.2. Intragranular microstructure

The principle constituent of the intragranular microstructure are rod-like β_1' precipitates, aligned parallel to the hexagonal axis. Representative micrographs showing different stages of the growth of the rods are provided in Figure 4. After 6 h ageing (Figure 4(a)) distribution of particle is sparse, with an average diameter of 6.2 ± 0.3 nm and a length of 65 ± 2 nm. (Estimates of the uncertainty are based on standard error of means measured over multiple regions of the same sample.) Precipitate length and diameter increased with ageing time and the number density of particles also increased substantially. After 406 h ageing diameter reaches 14 ± 2 nm and length 320 ± 20 nm. Samples aged for ≥ 24 h also contain plate-shaped β_2' precipitates with basal plane habit. A larger example of such plate-like precipitates can be seen in Figure 4(c). These precipitate are readily distinguishable from the rods by their orientation and stronger contrast, due to a greater thickness in the beam direction.

3.2.1. Precipitate size measurements Precipitate size distributions was determined from Monte Carlo simulations of the scattered x-ray intensity. There was little x-ray

---

‡ EBSD intensities are dimensionless values, and are scaled relative to the intensity for a random distribution (defined as 1.0).

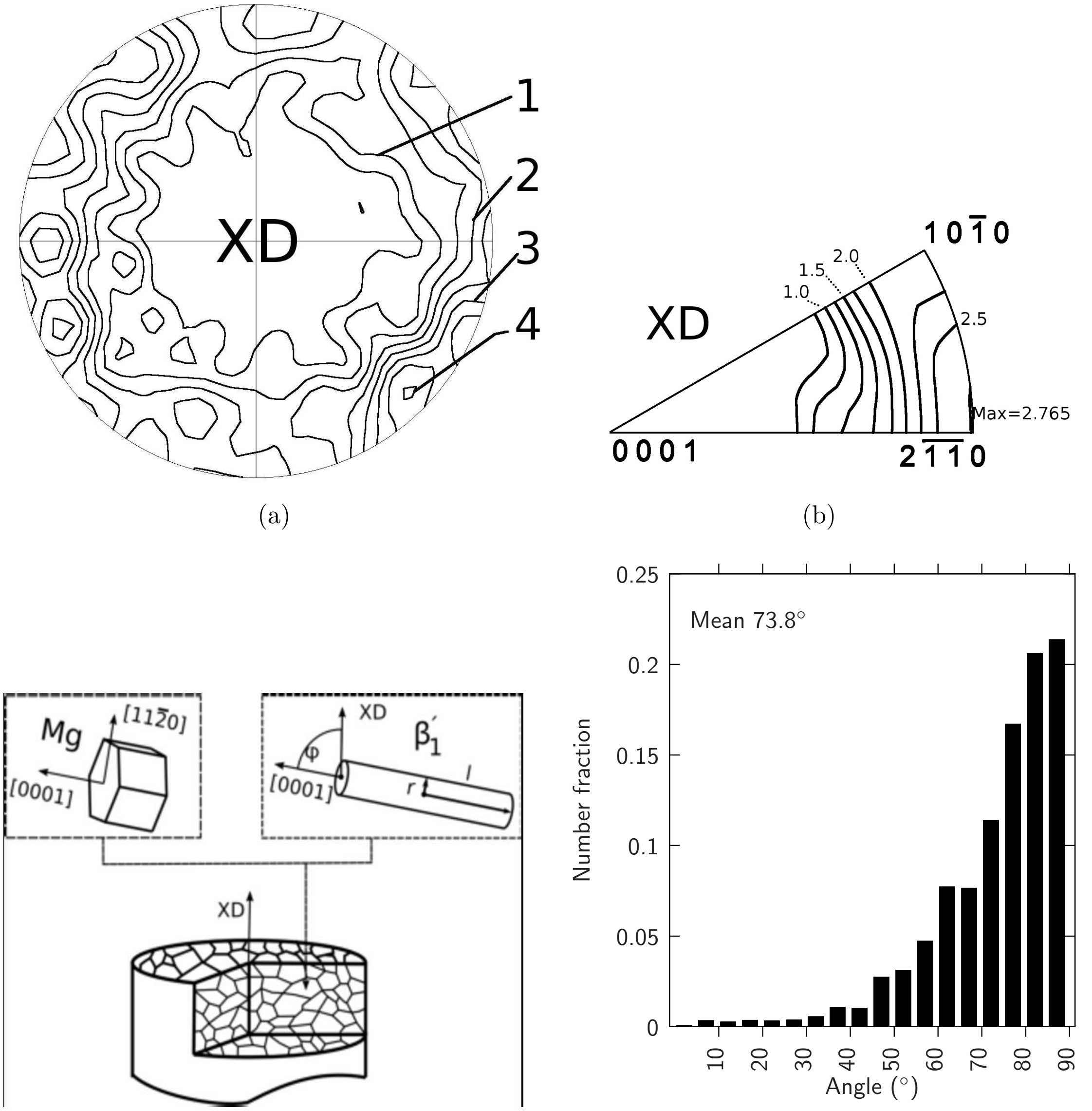

(a) (b)

(c) (d)

Figure 3. The texture of the extruded MgZn alloy. (a) Shows a stereographic pole figure obtained from electron back scattered diffraction (EBSD). Contours indicate the density of the distribution of $[0001]_{\mathrm{Mg}}$ poles. The [0001] poles are densest at the edges of the stereogram, i.e. almost perpendicular to the extrusion direction (XD). (b) Shows the corresponding inverse pole figure for the XD, showing that strongest texture component is for $(2\bar{1}\bar{1}0)$ plane normals. (c) Illustrates schematically the orientation of the β_1' precipitates relative to the extruded material. The long axis of the rods lies in the $[0001]_{\mathrm{Mg}}$ direction, at an angle φ to the XD. As shown by (a,b) the magnesium grains are commonly aligned with the [0001] direction radial and the $[2\bar{1}\bar{1}0]$ direction in the XD. (d) shows a frequency plot of the angle (φ) between the hexagonal axis of the Mg grains and the extrusion direction (XD) of the sample.

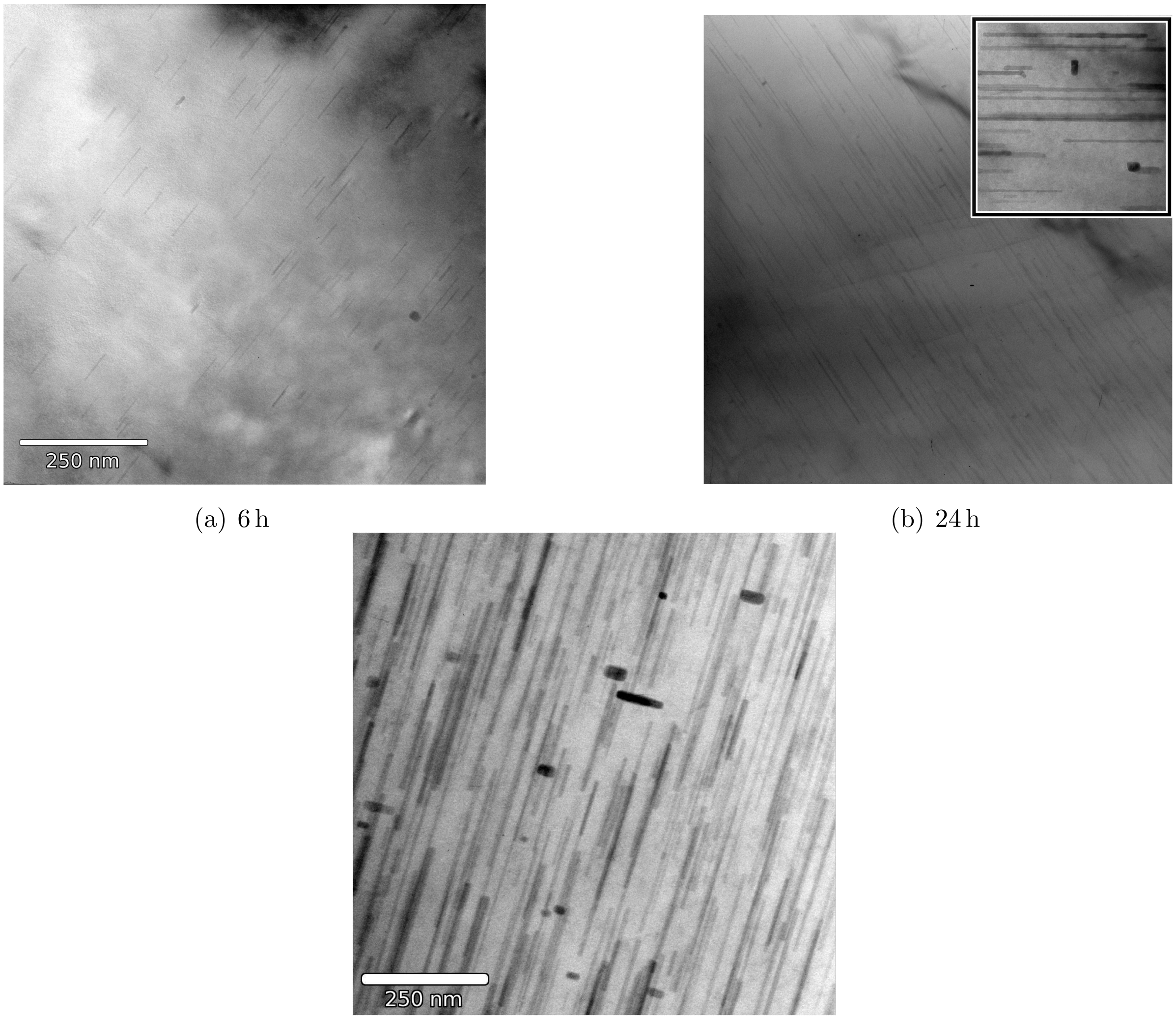

(a) 6 h

(b) 24 h

(c) 192 h.

Figure 4. Electron micrographs showing the size and number density of the rod-like β_1' precipitates after isothermal ageing time at 150°C for (a) 6 h, (b) 24 h and (c) 192 h.

scattering in the solution-treated and quenched sample (0 h ageing). The calculated precipitate size distribution is given in terms of volume-weighted particle radii in Figure 5. Since β_1' rods are not expected before ageing, the size distributions were determined for a spheroidal particles.

Isothermal ageing resulted in an increase in scattered intensity and a shift to larger precipitate sizes. The progressive changes in the precipitate size are shown in Figure 6 for SAXS (all ageing times) and TEM (6,24,192 and 406 h ageing). Measurements for both methods are expressed in terms of volume-weighed particle sizes. For SAXS data the ordinate is the volume fraction, whereas for TEM data it is given in arbitrary units. Aspect ratios measured in TEM were used in the Monte Carlo simulations. A value of 10 was used for 6 h ageing, and an aspect ratio of 20 for other ageing times.

The dominant feature in the SAXS data is a peak, initially centred at $\sim 3 \times 10^{-9}$ m and maximum volume fraction of 4.8×10^{-3}. This shifts to increasing particle size, reaching $\sim 7 \times 10^{-9}$ m at 406 h ageing. The intensity increases rapidly between 6 and 48 h ageing and more gradually for longer ageing times. The shoulder of a second peak can also be seen at higher precipitate radii. As with the major SAXS peak. this secondary peak increases in intensity with ageing time.

TEM data for precipitate radius and half-length are displayed in different colours below the respective SAXS plots. There is good agreement between the positions of the main SAXS peak and the precipitate radii measured in TEM. For ageing times of up to 192 h the precipitate half-lengths seem to co-incide with the position of the secondary SAXS peak, suggesting that this peak corresponds to the long axis of the rods, however, size range of the SAXS instrument ($r_{max} = 3.5 \times 10^{-8}$ m) is not sufficient to determine the position of the peak centre.

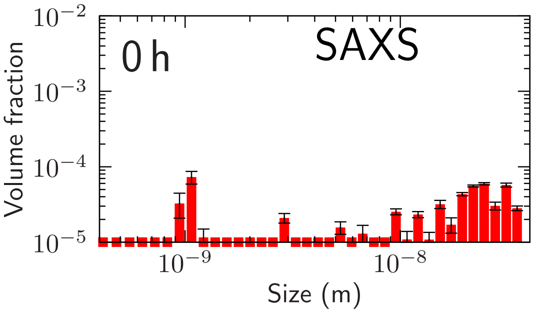

Figure 5. Volume-weighted SAXS particle size distributions for solution treated and quenched MgZn (h ageing). The distribution was calculated assuming spherical particles.

3.2.2. Precipitate volume fraction The β_1' precipitate volume fraction was determined from the SAXS measurements. The calculations were based on the β_1' precipitates being comprised of a mixture of the $MgZn_2$ Laves phase ($\rho = 5160$ Kg m^{-3}) and the Mg_4Zn_7 monoclinic phase ($\rho = 4800$ Kg m^{-3}). These phases have been shown to co-exist within the precipitates [22, 23]. Since the relative proportions of these phases have not been quantified, a 1:1 mixture of the two phases were assumed, giving a gravimetric density of 4960 Kg m^{-3}.

The volume fraction increase at a moderate rate up to 32 h, then undergoes a rapid increase between 32 h and 48 h ageing, as shown in Figure 7. The volume fraction continues to increase with further ageing and it appears that this process is still continuing up to at least 406 h ageing. The volume fraction after 406 h was 0.0283 ±0.0009, still substantially less than an estimate of a volume of ~0.035 based on the solubility of zinc at the ageing temperature.

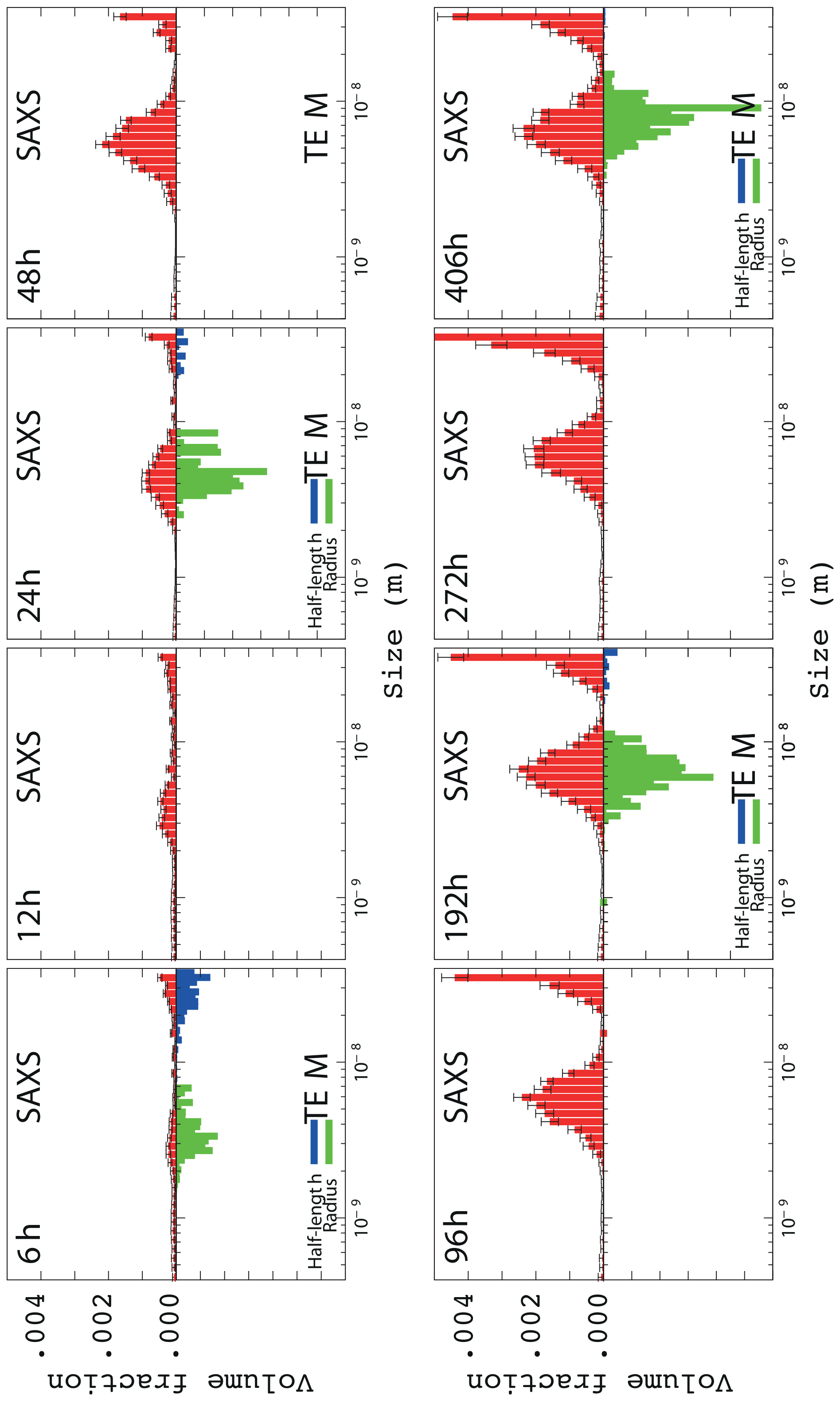

Figure 6. Volume-weighted SAXS and TEM particle size distributions for aged MgZn. The SAXS distributions were calculated assuming cylindrical rods of aspect ratio 10 (6 h) or 20 (all other samples).

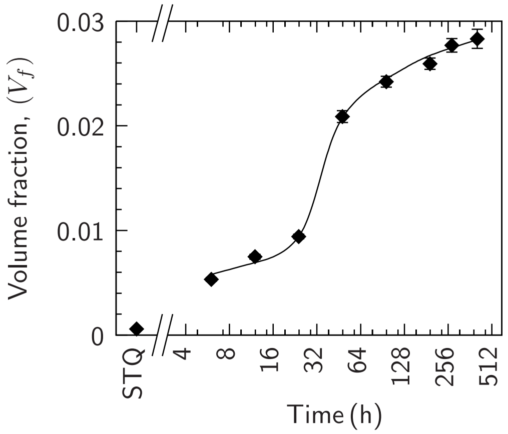

Figure 7. The volume fraction of β_1' precipitates as a function isothermal ageing time.

3.3. Mechanical properties

The alloy had a hardness value of 55 ±2 H_V in the solution-treated and quenched state (STQ) and reached a maximum value of 75±2 H_V after 96 h ageing. The change in hardness value with ageing time is shown in Figure 8. Error bars indicate the standard deviation in the hardness value, which was in the range of ±2 H_V. The hardness underwent a rapidly increase between 12 h and 96 h ageing, reaching a plateau at a value of 75±2 H_V. There was no further significant change in the hardness up to at least 406 h of ageing.

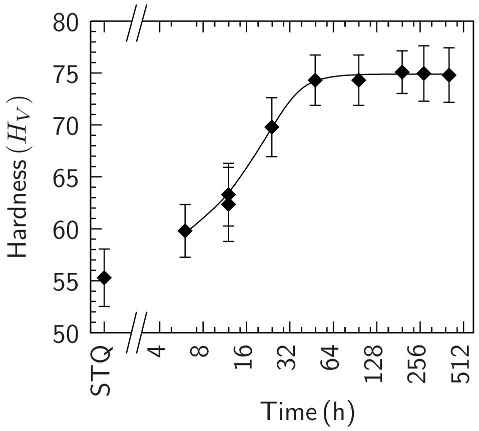

Figure 8. The microhardness of Mg-3.4at%Zn as a function of ageing time at 150 °C. Error bars indicate the standard deviation in each series of measurements. A dashed line has been included as a guide for the eye.

4. Discussion

SAXS measurements have the advantage of probing a volume that is orders of magnitude greater than TEM or atom probe. Based on a nominal SAXS beam diameter of 0.2 mm and a foil thickness of 0.6 mm each of the nine measurements reported in this work covered a volume of approximately 0.02 mm^3. In this context it is worth noting that the total volume of material analysed in all TEMs worldwide up to 1996 has been estimated at 1 mm^3.

The Monte Carlo technique provides the possibility of obtaining physically representative size data from anisotropic precipitates, provided that information on the morphology and orientation of the scattering sites is known. A knowledge of the alloy texture, combined with TEM observations of the microstructure provided the information necessary to analyse the SAXS data with the rod-like particles modelled as high aspect-ratio cylinders.

Anisotropic precipitates can be divided into three categories; This work examined rod-like precipitates, which were described by two parameters: r_1 and r_2 with $r_1 \gg r_2$. There are also many examples of plate-like precipitates for which $r_2 \gg r_1$. Lath-like precipitates are also formed in some systems and require three parameters to describe the size; r_1, r_2, r_3 with $r_3 > r_2 > r_1$.

To extract physically representative information about anisotropic precipitates it is necessary to perform the experiments in such a way that scattering from radial components $r_1 \ldots r_n$ can be distinguished. In the case of precipitates phases in polycrystalline metals this can be divided into two separate issues; the relationship between the beam and the matrix and secondly the relationship between the matrix and the precipitate.

In a single-crystal the orientation of the beam with respect to the matrix can be controlled via alignment of the bulk sample. However, for a polycrystal it is essential to consider not only the alignment of the sample but also the texture of the material. The low spatial resolution of SAXS results in scattering being averaged over a considerable volume. In a randomly textured material this will generally result in sampling a sufficient number of grains that scattering becomes isotropic, making it impossible to extract physically representative 2-D data from small-angle scattering. In this work the alloy was extruded in order to develop texture, ensuring that precipitate length data was not convoluted with precipitate radius data.

Secondly it is important to consider the orientation the precipitates with respect to the grains. Many semi-coherent precipitates possess a simple, rational orientation relationship with the matrix. These arise in order to minimise the energy barrier to nucleation of the precipitates and there is an extensive body of literature concerned with the prediction of orientation relationships.

The case of $\langle 0001 \rangle$ rods in Mg relatively simple because a unique axis of the precipitate lies parallel to a unique axis of the matrix. In general a number of crystallographically equivalent variants of a precipitate phase will exist for a given orientation relationship. For example, there are three crystallographic equivalents of prismatic plane plates in Mg. Other difficulties will arise where a precipitate is able to adopt more than one orientation relationship with the matrix, often resulting in precipitates of a single phase, but differing morphologies (eg MgSn). Such complications would make extracting data difficult and a detailed understanding of the texture would be essential.

In some instances it may not be practical to obtain 2-D due to the presence of multiple phases. This study focused on the size and volume fraction of the β_1' phase, which is the majority precipitate phase in MgZn alloys. Plate-like precipitates with (0001) habit were also observed and micrographs show that these precipitates have a size range which falls within the range of measurements for β_1' particles. This makes it impossible to distinguish between the two phases in scattering measurements, however, the supporting TEM images shows that this phase is only a very minor constituent and unlikely to substantially influence the results. In general it is possible for two or more precipitates of different phases with similar sizes to be present at a given ageing time. The presence of non-stoichiometric phases would make quantification of the volume fraction impractical, since these calculations require a known density for each phase.

The use of complementary SAXS and TEM has great potential for characterizing precipitate-strengthened alloys. The Monte Carlo SAXS technique makes it possible to obtain physically representative measurements of particles with two independent size parameters, such as precipitate rods or plates. This requires *a priori* information on the precipitate morphology and crystalline habit, which is readily available through TEM. Combined with a knowledge of the material texture, for example through EBSD analysis, this data makes if possible to rapidly meaningful stereographic information from sample volumes orders of magnitude greater than with TEM.

A purpose-built SAXS apparatus is currently under construction and will extend the range of particle sizes from the current limit of 35 nm to $\sim 1\mu$m. This instrument will greatly extend the utility of SAXS particle size measurements, making it possible not only to measure large isotropic particles but also to simultaneously measure two size parameters in high aspect ratio precipitates, e.g. rod length and diameter in MgZn alloys.

5. Conclusion

The precipitation behaviour of a MgZn alloy has been examined in detail, clearly demonstrating the value of using complementary TEM and SAXS for the analysis of anisotropic precipitates.

A MgZn alloy was textured through extrusion and the orientation of the grains measured by EBSD. The precipitate morphology was observed using diffraction contrast TEM. This made it possible to relate the orientation of the bulk sample to that of the principle scattering sites. These provided the information necessary for SAXS analysis by Monte Carlo simulation, making it possible to quantify precipitate size and number density for anisotropic rod-like precipitates.

Acknowledgments

The authors would like to express their thanks to Dr. Hidetoshi Somekawa who extruded the material used in this work and collected the EBSD data and to Dr Pavel Kowalski for assistance with the SAXS measurements.

References

[1] P. Bardhan and A. Starke, Jr. Preprecipitation in Al/Zn/Mg Alloys Studied by Hardness and Small-Angle X-ray Scattering Measurements. *J. Mater. Sci*, 3(6):577–583, 1968.

[2] A. Deschamps, A. Bigot, F. Livet, P. Auger, Y. Brechet, and D. Blavette. A comparative study of precipitate composition and volume fraction in an Al-Zn-Mg alloy using tomographic atom probe and small-angle X-ray scattering. *Philos. Mag. A*, 81:2391–2414, 2001.

[3] A. Deschamps, F. Livet, and Y. Bréchet. Influence of predeformation on ageing in an Al-Zn-Mg alloy–i. microstructure evolution and mechanical properties. *Acta Mater.*, 47(1):281–292, 1999.

[4] A. Dubey, B. Schöofeld, and G. Kostorz. Shape and internal structure of Guinier-Preston zones in Al-Ag. *Acta Metall. Mater.*, 36(6):1161–1170, 1991.

[5] R. Erni, H. Heinrich, and G. Kostorz. On the internal structure of Guinier-Preston zones in Al-3 wt.% Ag. *Philos. Mag. Lett.*, 83(10):599–609, 2003.

[6] A. Malik, B. Schoenfeld, G. Kostorz, W. Buehrer, and J. S. Pedersen. Early stages of decomposition in Al-Ag and Al-Cu. *Z. Metallkd.*, 88:625–629, 1997.

[7] B.A. Pletcher, K.G. Wang, and M.E. Glicksman. Experimental, computational and theoretical studies of δ' phase coarsening in Al-Li alloys. *Acta Mater.*, 60(16):5803–5817, 2012.

[8] AJ Allen, D Gavillett, and JR Weertman. Sans and tem studies of isothermal m2c carbide precipitation in ultrahigh strength af1410 steels. *Acta Metall Mater*, 41(6):1869–1884, Jan 1993.

[9] A. W. Zhu, B. M. Gable, G. J. Shiflet, and E. A. Starke, Jr. The intelligent design of age hardenable wrought aluminum alloys. *Adv. Eng. Mater.*, 4(11):839–846, 2002.

[10] J. F. Nie, B. C. Muddle, and I. J. Polmear. The effect of precipitate shape and orientation on dispersion strengthening in high strength aluminium alloys. In J. H. Driver, F Dubost, B; Durand, R Fougeres, P Guyot, P Sainfort, and M Suery, editors, *Mater. Forum*, volume 217, pages 1257–1262, 1996.

[11] J. F. Nie. Effects of precipitate shape and orientation on dispersion strengthening in magnesium alloys. *Scr. Mat.*, 48:1009–1015, 2003.

[12] P Fratzl. Small-angle scattering in materials science - a short review of applications in alloys, ceramics and composite materials. *Journal of Applied Crystallography*, 36:397–404, 2003.

[13] A. D. Sequeira, G. Kostorz, and J. S. Pedersen. Small-angle neutron scattering from anisotropic single-crystalline materials. *Journal of Applied Crystallography*, 30:575–579, 1997.

[14] J. S. Pedersen. Analysis of small-angle scattering data from colloids and polymer solutions: modeling and least-squares fitting. *Advances in Colloid and Interface Science*, 70:171–210, 1997.

[15] B. R. Pauw, J. S. Pedersen, S. Tardif, M. Takata, and B. B. Iversen. Improvements and considerations for size distribution retrieval from small-angle scattering data by monte-carlo methods. Available on arXiv, submitted to J. Appl. Cryst., 10 2012.

[16] L. Sturkey and J. B. Clark. Mechanism of age-hardening in magnesium-zinc alloys. *J. Inst. Mater.*, 88:177–181, 1959-60.

[17] J. B. Clark. Transmission electon microscopy study of age hardening in a Mg-5wt.%Zn alloy. *Acta Metall.*, 13:1281–1289, 1965.

[18] J. M. Rosalie, Hidetoshi Somekawa, Alok Singh, and Toshiji Mukai. The effect of size and distribution of rod-shaped precipitates on the strength and ductility of a Mg-Zn alloy. *Mater. Sci. Eng. A*, 539:230–237, 2012.

[19] P. Kraft, A. Bergamaschi, Ch. Brönnimann, R. Dinapoli, E. F. Eikenberry, B. Henrich, I. Johnson, A. Mozzanica, C. M. Schlepuetz, P. R. Wilmott, and B. Schmitt. Performance of single-photon-counting pilatus detector modules. *Journal of Synchrotron Radiation*, 16:368–375, 2009.

[20] E. F. Eikenberry, Ch. Brönnimann, G. Hülsen, H. Toyokawa, R. Horisberger, B. Schmitt, C. Schulze-Briese, and T. Tomizaki. Pilatus: a two-dimensional x-ray detector for macromolecular crystallography. *Nucl Instrum Meth A*, 501(1):260–266, Jan 2003.

[21] Fan Zhang, Jan Ilavsky, Gabrielle G Long, John P. G Quintana, Andrew J Allen, and Pete R Jemian. Glassy carbon as an absolute intensity calibration standard for small-angle scattering. *Metall Mater Trans A*, 41A(5):1151–1158, Jan 2010.

[22] Julian M. Rosalie, Hidetoshi Somekawa, Alok Singh, and Toshiji Mukai. Structural relationships among $MgZn_2$ and Mg_4Zn_7 phases and transition structures in Mg-Zn-Y alloys. *Philos. Mag.*, 90(24):3355–3374, 2010.

[23] A. Singh, J. M. Rosalie, H. Somekawa, and T. Mukai. The structure of precipiates in Mg-Zn-Y alloys. *Philos. Mag. Lett.*, 90, 2010.